Comparison of nanobridge lithography techniques for nanoscale SQUID devices

Jamie A. Potter, Gemma Chapman, Tom Godfrey, Laith Meti, Parth Bhandari, Olena Shaforost, John Gallop, Gustavo Trindade, Ian Gilmore, Christopher Chunnilall, Simon Hall, Xue Shen Wang, Qing Zhong, Jin Jin Li, David Cox, Ed Romans, and Ling Hao

***Abstract*—NanoSQUIDS incorporating nanobridges as the Josephson element are desirable since their small dimensions mean they can be situated in close proximity to very small, highly localised magnetic moments for high spin sensitivity. Key to achieving the necessary dimensions are the lithographic technologies used to fabricate the nanobridges. Here we present characterisation of Nb nanoSQUIDs incorporating nanobridges fabricated by three different techniques: neon focused ion beam (FIB) lithography, gallium FIB lithography and e-beam lithography (EBL). We discuss the critical currents and voltage-current characteristics achieved by each technique at various temperatures for a range of nanobridge widths, and discuss the corresponding nanoSQUID voltage modulation and potential applications.**

***Index Terms*—Superconducting Quantum Interference Device (SQUID), nanoSQUID, nanobridge, weak links, focused ion beam (FIB) lithography, electron beam lithography (EBL).**

I. INTRODUCTION

NANOSQUIDS have been used in a variety of nanoscale magnetic particle detection experiments due to their unrivalled sensitivity to magnetic flux [1-8]. For a fundamental magnetic dipole such as that associated with electron spin, most of the magnetic flux is concentrated near to the spin [9], and therefore strongly coupling such a flux to a SQUID loop becomes a challenging task. To achieve a high spin sensitivity $\sqrt{S_B}$ requires both optimal coupling and a low equivalent flux noise $\sqrt{S_\Phi}$ (which decreases with temperature). This requires fabricating as small a SQUID as possible with a low inductance – a nanoSQUID. In the regime of temperature being much lower than the plasma frequency of the nanoSQUID, the sensitivity is expected to approach the standard quantum limit [10].

Commonly used oxide-layer Josephson junctions are generally unsuitable for achieving the smallest nanoSQUIDs, as their low critical current density means junction areas must be on the order of microns. Some groups have developed novel tunnel junction technologies to help address this [2,3] or investigated novel alternatives such as carbon nanotubes coupled to superconducting electrodes [11] or devices fabricated on quartz tips [12]. But perhaps the simplest approach is to use nanobridge weak links fabricated from a single layer of superconducting thin film, with dimensions of order the Ginzburg-Landau coherence length $\xi_{GL}(T)$ (~ 40 nm for Nb at 4.2 K). A number of techniques have been demonstrated to fabricate such nanobridges including electron-beam lithography (EBL) [9,13-18] and focused ion beam (FIB) milling with different ion species [16,19-21]. However, there are several considerations when using nanobridges, and the most appropriate technique to fabricate them can depend on the intended application and the desired operating temperature regime.

The first issue is that the coherence length itself decreases with decreasing temperature, and to maintain a single-valued current-phase relation requires the bridge length $l < 3.5\ \xi_{GL}(T)$ [22] which means shorter bridges are required for lower temperature operation, placing more stringent requirements on the fabrication process. The second issue, particularly for devices with larger critical currents is that when nanobridges are operated in the voltage state, Joule heating can lead to undesirable hysteretic *V(I)*-characteristics due to hotspot formation when the current to self-sustain the hotspot is lower that the critical current I_c [23,24]. This means techniques such as FIB that can produce smaller critical currents are often desirable. Smaller critical currents are also desirable where the nanobridge is instead operated with dispersive readout as a non-linear inductor, since the Josephson inductance $L_J \propto I_c^{-1}$. The third issue is that continued progress in quantum technologies requires the development of scalable nanoSQUID sensors, as

Date of submission: 1st October 2025. This work was supported by the UK Science and Technologies Funding Council (STFC) via grants ST/T006064/1 & ST/T006099/1 (Quantum Sensors for the Hidden Sector) and ST/T006137/1 (Quantum Technologies for Neutrino Mass); by the UK Department for Science, Innovation and Technology (DSIT) through the National Measurement System (NMS), the National Quantum Technologies Programme (NQTP), and the Government Office for Technology Transfer (GOTT); and by the National Natural Science Foundation of China (61701470). *(Corresponding author: Ed Romans (e.romans@ucl.ac.uk).)*

Jamie A. Potter, Gemma Chapman, Laith Meti, Olena Shaforost, John Gallop, Gustavo Trindade, Ian Gilmore, Christopher Chunnilall, Simon Hall, and Ling Hao are with the National Physical Laboratory, Teddington, TW11 0LW, UK.

Tom Godfrey, Laith Meti, Parth Bhandari and Ed Romans are with the London Centre for Nanotechnology, University College London, London, WC1H 0AH, UK.

Xue Shen Wang, Qing Zhong, and Jin Jin Li are with the Centre for Advanced Measurement Science, National Institute of Metrology, Beijing, 100029, China.

David Cox is the with Advanced Technology Institute, University of Surrey, Guildford, GU2 7XH, UK.

for example in a recent proposal for a spin-based quantum computer [25], which describes a large array of magnetic sensors in close proximity to a qubit layer. Such a scheme could be realized with a nanoSQUID array, and therefore the fabrication technique should be scalable with high throughput. Currently, the only realistic solution to achieve these requirements is the fabrication of nanoSQUIDs by EBL.

With that in mind, in this paper we present the detailed development of a single step EBL process, which was used to fabricate nanoSQUIDs from a single layer of Nb, in a single lithography step. Loop diameters down to 150 nm have been achieved, together with nanobridge dimensions as small as 25 nm wide x 60 nm long. We present DC characterisation of a typical Nb nanoSQUID fabricated by this approach, and compare the critical currents achieved with similar devices fabricated by Ga or Ne FIB. The nanoSQUID flux modulation is also characterised, revealing a large voltage-to-flux conversion, indicating suitability of these nanoSQUIDs for achieving low flux noise operation.

II. Fabrication Details

Our nanoSQUIDs are fabricated from a single 150 nm-thick layer of niobium, deposited by dc magnetron sputtering onto a 525 μm-thick, 4" wafer of thermally oxidized silicon. Prior to lithography, the wafer is diced into 10 mm x 10 mm chips, which are then cleaned by sonicating in acetone, de-ionised water, and finally isopropanol (IPA). The resulting chips are measured to have a T_c of 9 K that is consistent to within ~ 0.1 K for samples taken from different parts of the wafer, excluding the region of ~ 10 mm around the edge. For devices with EBL nanobridges the entire chip design is written in a single EBL processing step. For devices with Ne or Ga FIB nanobridges we first define the larger features and nanoSQUID loop by EBL followed by separate FIB milling of the nanobridges.

In our EBL process, a 300 nm-thick layer of poly-methyl methacrylate (PMMA) resist is first spin-coated on to the chip at 2.5 krpm, and given a pre-exposure bake at 180°C for 90 s. Immediately following coating, a 100 keV electron-beam is then used to pattern the SQUID circuit, using the PMMA as a positive-tone resist. The leads and contacts are exposed with a beam current of 40 nA and a dose of 1 mC/cm^2. A beam current of 1 nA is used to expose the nanoSQUIDs, giving a nominal beam spot size at the top surface of the resist of 2.5 nm. A base dose of 900 μC/cm^2 is modified by a proximity-effect correction calculation [26], in order to ensure small features such as the nanoSQUID loop are fully exposed. Following exposure, the resist is developed for 60 s in a 1:3 solution of methyl isobutyl ketone (MIBK) and IPA, at room temperature.

The EBL pattern is transferred into the Nb film by reactive-ion etching (RIE) using a 2:5 volume ratio of CHF_3 and SF_6, at a gas pressure of 100 mbar and a power of 100 W. The PMMA resist has relatively poor etch resistance, etching approximately twice as quickly as the underlying Nb film and necessitating the use of a relatively thick resist layer. Finally, the remaining resist is removed by sonicating in an acetone bath at 65°C, and plasma ashing in oxygen for 2 minutes.

To fabricate devices with Ne FIB nanobridges we use a Ne beam accelerated by an energy of 20 keV, focused to a spot at the surface of the chip which is indirectly measured to be 15 nm in diameter. A dose of 2.5 nC/μm^2 is sufficient to clear the Nb film. Using this method, nanobridges down to 50 nm wide x 30 nm long can be fabricated, somewhat shorter than with the EBL method. To fabricate devices by Ga FIB we use a dual-beam FIB system where a layer of amorphous tungsten is deposited over the film where the nanobridges are to be placed, using e-beam decomposition of $W(CO)_6$. This provides both protection of the Nb film against Ga ion implantation damage and a normal metal shunt resistor for each bridge.

An example of a nanoSQUID fabricated solely by EBL is shown in the top panel of Fig.1. This nanoSQUID has a loop diameter of 150 nm, and has nanobridges of approximately 40 nm wide x 60 nm long. The narrowest nanobridge width we have successfully fabricated by this positive-tone PMMA EBL method is 25 nm which is limited by the long-chain molecular structure of PMMA, and the minimum achieved length is 60 nm, limited by broadening of the electron beam due to scattering in the resist.

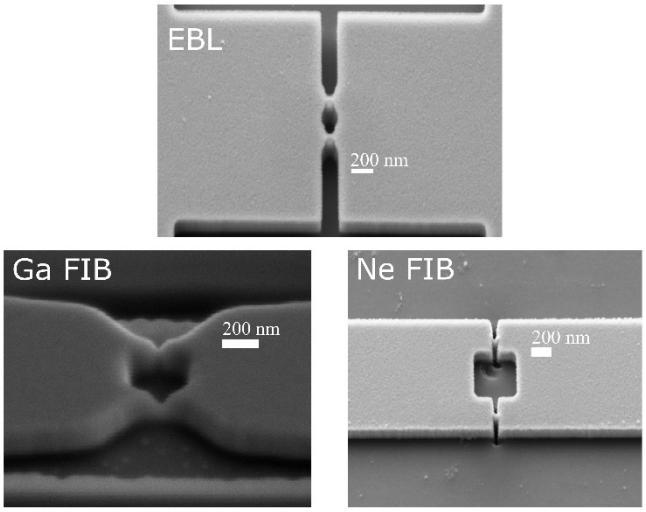

Fig. 1. Top: SEM image of a Nb nanoSQUID with loop diameter 150 nm, fabricated by a single-step positive-tone PMMA EBL process. Bottom: examples of Nb nanoSQUIDs with the nanobridges instead fabricated by Ga FIB (left) or Ne FIB (right). (Note the images are not to the same scale.)

III. Results and Discussion

A. V(I) Characterisation

A nanobridge weak link can support a supercurrent up to a critical current I_c, above which it enters the voltage state where a time-dependent, non-zero voltage develops across the bridge. As with a tunnel junction, a nanobridge may exhibit hysteresis in its current versus time-averaged voltage characteristic. In a tunnel junction, this is due to the intrinsic capacitance and high normal state resistance of the junction, but in a nanobridge the capacitance is negligible and the normal state resistance is much lower. Instead, the usual explanation, as previously mentioned, is that the hysteresis arises as a result of hotspot formation –

Joule heating causes a region of elevated temperature extending into the banks, which remains even after the bias current has been reduced below I_c. A further possible explanation at low temperatures, or for bridges where the requirement $l < 3.5\,\xi_{GL}(T)$ is not satisfied, is that the nanobridge is exhibiting a multi-valued current-phase relation (CPR), depending on the bridge geometry where Josephson-like behaviour is replaced by a one-dimensional depairing effect involving phase slippage and vortex motion [22,27,28].

The $V(I)$ curve, as a function of sample temperature, for an EBL nanoSQUID with EBL nanobridge dimension of 25 nm x 60 nm is shown at the top of Fig. 2. We see a critical current which increases with decreasing temperature, going from approximately 50 μA at 8 K, to 500 μA at 3.5 K (the base temperature of the measurement system). A resistively-shunted junction (RSJ)-like behaviour emerges below around 6.5 K, but with a noticeable region of high differential resistance dV/dI just above I_c. At 4 K and below, the nanoSQUID $V(I)$ is beginning to exhibit some hysteresis. This is most likely due to hotspot formation, given the fairly large I_c and the fact that the dissipated power above I_c is 5 times larger at 3.5 K than it is at 6 K. A cross-over to a multi-valued CPR for Nb nanobridges was reported in [28] for a similar temperature regime, but the nanobridges in that work had much lower critical currents and higher normal state resistances than for our nanobridges. A further investigation to distinguish between the two potential causes of hysteresis would still be beneficial, either by direct measurement of the CPR as in [28], or by the addition of a thin gold capping layer as in [9] which would shift the onset of hysteresis to a lower temperature if it is caused by a hotspot.

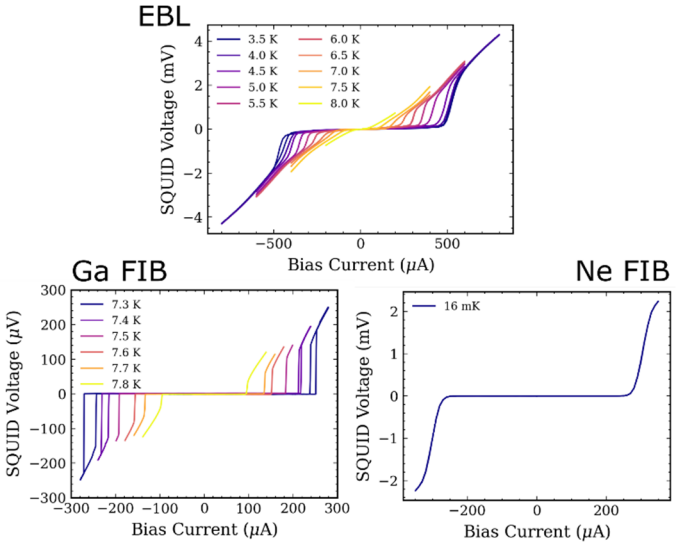

Fig. 2. $V(I)$ characteristics of nanoSQUIDs incorporating different types of nanobridge weak links. Top: EBL device with nanobridges of dimensions 25 nm wide x 60 nm long, measured at temperatures varying from 3.5 K up to 8 K. Bottom left: Ga FIB device with nanobridge dimensions of 50 nm wide x 30 nm long, measured at temperatures varying from 7.3 K up to 7.8 K. Bottom right: Ne FIB device with nanobridge dimensions of 25 nm wide x 60 nm long, measured at a temperature of 16 mK.

A detailed comparison of the temperature dependence of the critical currents achieved for similar sized nanoSQUIDs incorporating either EBL, Ga FIB, or Ne FIB nanobridges is shown in Fig. 3. As can be seen Ga FIB and especially Ne FIB produce much smaller critical currents than EBL for nominally the same nanobridge width as seen under an SEM. Such differences can be partly explained by the expected lateral implantation of ions into the nanobridge structure in the FIB process that can suppress T_c [6,16,19], but also, as can be seen in Fig. 1, because the FIB nanobridges tend to be thinner than the surrounding superconducting bank and the thin film.

As can be seen in Fig. 3 both the EBL and FIB devices have some spread in the critical currents even for the widest EBL nanobridges. We see similar spreads for each technique both for devices on the same chip and also between chips. This is perhaps not surprising for FIB devices because FIBs are more manual tools with each nanobridge etched individually. For the more automated EBL process we find the typical on-chip variation in critical currents of nanobridges is reasonably small ~17% and probably accounted for by slight variations in nanobridge dimensions as-fabricated.

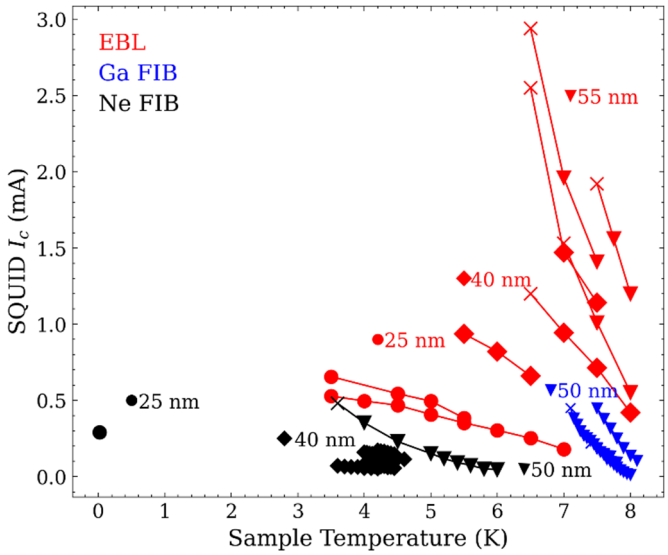

Fig. 3. Comparison of the temperature-dependence of the nanoSQUID critical current for nanoSQUIDs incorporating either EBL (red), Ga FIB (blue), and Ne FIB (black) nanobridges. All of the measurements were performed in a cryocooler with a base temperature of 3-4 K apart from the single Ne FIB measurement on the left-hand side of the figure which was performed in a dilution fridge at 16 mK. Across all devices the loop size and the nanobridge length was kept the same, but the nanobridge width was varied as indicated by the legend. Solid symbols show non-hysteretic measurements and crosses show measurements of the critical current where the $V(I)$ curve started to display hysteresis as the temperature was lowered. Further measurements were generally not taken at lower temperatures than this. In some of the EBL measurements the base temperature of the system was not sufficient to reach the hysteretic regime.

Although not easily visible in the figure, for Ne FIB the critical currents at 4.25 K are spread from about 50 to 300 μA with four of the measured devices being clustered well below 180 μA, and the fifth device being an outlier at 300 μA. The Ne FIB device with 25 nm wide nanobridges was also measured at a much lower temperature of 16 mK and the $V(I)$ curve is shown in Fig. 2 showing an absence of hysteresis, in contrast to the typical behaviour seen in the EBL devices.

The temperature dependence of the critical current $I_c(T)$ just below T_c varies between devices. For narrow bridges we see a generally linear dependence close to T_c tending to a shallower gradient dI_c/dT as $T \rightarrow 0$ which agrees with the theoretical prediction of the Kulik-Omelyanchuk (KO-1) model for short, one-dimensional dirty metallic weak links [22]. In contrast wider FIB nanobridges deviate from this with a more convex shape close to T_c more suggestive of a superconductor-normal metal-superconductor (S-N-S) structure [22]. Similar behaviour has been reported for instance in [16] for Ga FIB junctions. Since our nanobridges are unlikely to be in the long junction limit (where the nanobridge length, $l >> \xi_{GL}(T)$) the most likely explanation is that the behaviour we observe is related to ion implantation during FIB milling leading to a small normal region in the nanobridge structure.

B. Flux modulation

The flux modulation $V(\Phi)$ curves of the nanoSQUIDs fabricated by the different techniques were measured by placing the chip within the bore of a superconducting solenoid magnet and applying a global magnetic field perpendicular to the surface of the chip. Fig. 4 shows the change in nanoSQUID output voltage as a function of applied flux Φ_{ext} for different values of the nanoSQUID bias current just above the respective critical current. The EBL and Ga FIB devices are operated just below T_c in the regime where they have non-hysteretic behaviour. The Ne FIB device is shown at 16 mK since it still displayed non-hysteretic behaviour at such low temperature. We observe the expected periodic modulation of the output voltage for each type of device.

For the EBL device, shown at the top of Fig. 4, the magnetic field period ΔB is 250 μT, giving an effective area of the nanoSQUID of $A = \Phi_0/\Delta B = 8.4$ μm^2. This is significantly larger than the geometric area of the nanoSQUID, which we attribute to flux-focussing by large areas of Nb surrounding the nanoSQUIDs following patterning. Similar flux-focussing behaviour was seen for other devices although the field periods were not identical due to differences in loop sizes. The steepness of the $V(\Phi)$, relates directly to the sensitivity of the nanoSQUID. In this case for the EBL device at 5.5 K we find a maximum voltage-to-flux transfer coefficient of V_Φ = 2.6 mV/Φ_0, at a bias current of 225 μA and an applied flux of 0.2 Φ_0. The Ga FIB device has a much lower modulation depth and transfer function, V_Φ = 0.5 mV/Φ_0, because the device had to be operated closer to T_c for non-hysteretic $V(I)$ behaviour.

It is interesting to compare the EBL device to the $V(\Phi)$ curve at 16 mK for the nanoSQUID with Ne FIB. This has a larger V_Φ = 10 mV/Φ_0 than the EBL nanobridge device measured at the much higher temperature. For ideal nanoSQUIDs with similar loop inductances and nanobridge critical currents, the transfer function might be expected to depend on the I_cR_n product and thus the normal resistance R_n of the nanobridges. For the EBL nanobridges we estimate R_n = 8.8 Ω and for the Ne FIB nanobridges we estimate R_n = 12.5 Ω from the RSJ-model fitted to the data. The approximately four times larger transfer function of the Ne FIB device compared to the EBL device is only partly explained by these estimates. One possible explanation is that, as previously mentioned, the Ne FIB nanobridges tend to have a region of high dV/dI just above I_c leading to very steep $V(\Phi)$ curves when biased in this region as can be seen in the shape of the curves in Fig. 4. The high dV/dI may be due to the details of the poisoning profile close to the junction [29] or other non-ideal weak-link behaviour [22]. Further investigation of this and how it differs between EBL and Ne FIB nanobridges is ideally required to understand the sensitivity differences between the devices.

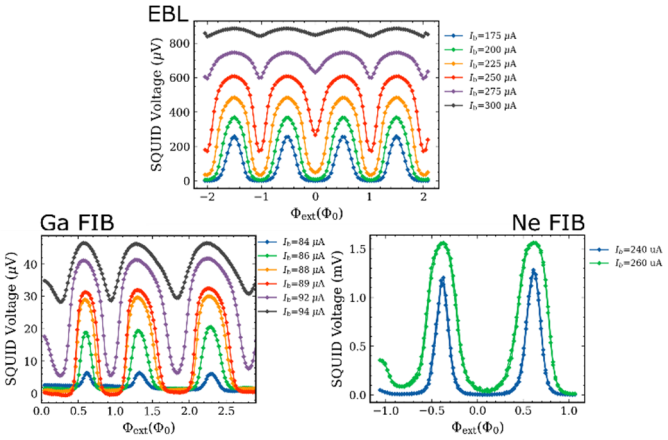

Fig. 4. Flux modulation $V(\Phi)$ of nanoSQUIDs incorporating different types of nanobridge weak links for various bias currents I_b above their respective critical currents. Top: EBL device with loop diameter 150 nm, and nanobridge dimensions 25 nm wide x 60 nm long, measured at a temperature of 5.5 K. Bottom left: Ga FIB device with loop diameter 300 nm, and nanobridge dimensions of 50 nm wide x 30 nm long, measured at a temperature of 7.8 K. Bottom right: Ne FIB device with loop diameter of 150 nm, and nanobridge dimensions of 25 nm wide x 60 nm long, measured at a temperature of 16 mK.

IV. Summary

In summary we have demonstrated the successful fabrication of nanoSQUIDs incorporating nanobridges fabricated by EBL or Ga/Ne FIB. Both EBL and Ne FIB devices show high voltage modulation making them useful for highly sensitive flux measurements. EBL nanobridges generally have much larger critical currents and are only hysteresis free at higher temperatures which makes them only suitable for conventional voltage state readout at these higher temperatures. However, the versatility and fast processing speed of EBL favours EBL nanobridges for the development of wafer-scale devices. Ne FIB devices in contrast have lower critical currents and may be favoured for more bespoke individual devices designed for ultimate sensitivity at mK temperatures.

REFERENCES

[1] C. P. Foley, and H. Hilgenkamp, "Why nanoSQUIDs are important: an introduction to the focus issue", *Supercond. Sci. Technol*. 22, 064001, 2009, doi: 10.1088/0953-2048/22/6/064001.

[2] M. J. Martínez-Pérez *et al.*, "Three-Axis Vector Nano Superconducting Quantum Interference Device", ACS Nano 10, pp. 8308-8315, 2016, doi: 10.1021/acsnano.6b02218.

[3] M. Schmelz et al., "3D nanoSQUID based on tunnel nano-junctions with an energy sensitivity of 1.3 *h* at 4.2K", *Appl. Phys. Lett.* 111, 032604, 2017, doi: 10.1063/1.4986655.

[4] C. Granata and A. Vettoliere, "Nano Superconducting Quantum Interference device: A powerful tool for nanoscale investigations", *Phys. Rep*. 614, pp. 1–69, 2015, doi: 10.1016/j.physrep.2015.12.001.

[5] L. Hao and C. Granata, "Recent trends and perspectives of nanoSQUID: introduction to 'Focus on nanoSQUIDs and their applications'", *Supercond. Sci. Technol.* 30, 050301, 2017, doi: 10.1088/1361-6668/aa68d6.

[6] A. G. P. Troeman *et al.*, "NanoSQUIDs Based on Niobium Constrictions", *Nano Lett.* 7(7), pp. 2152-2156, 2007, doi: 10.1021/nl070870f.

[7] W. Wernsdorfer, "From micro- to nano-SQUIDs: applications to nanomagnetism", *Supercond. Sci. Technol*. 22, 064013, 2009, doi: 10.1088/0953-2048/22/6/064013.

[8] M. I. Faley *et al*., "TiN nanobridge Josephson junctions and nanoSQUIDs on SiN-buffered Si", *Supercond. Sci. Technol.* 35, 065001, 2022, doi: 10.1088/1361-6668/ac64cd.

[9] S. K. H. Lam and D. L. Tilbrook, "Development of a niobium nanosuperconducting quantum interference device for the detection of small spin populations", *Appl. Phys. Lett*. 82, pp. 1078–80, 2003, doi: 10.1063/1.1554770.

[10] J. Clarke and A. I. Braginski (Eds.), *The SQUID Handbook Vol. 1*, Weinheim: Wiley–VCH, GmbH and Co. KGaA, 2004.

[11] J. -P. Cleuziou *et al*., "Carbon nanotube superconducting quantum interference device", *Nature Nanotech* 1, pp. 53–59, 2006, doi: 10.1038/nnano.2006.54.

[12] A. Finkler *et al*., "Self-Aligned Nanoscale SQUID on a Tip", *Nano Lett.* 10(3), pp. 1046-1049, 2010, doi: 10.1021/nl100009r.

[13] K. Hasselbach, D. Mailly and J. R. Kirtley, "Micro-superconducting quantum interference device characteristics", *J. Appl. Phys.* 91, pp. 4432-4437, 2002, doi: 10.1063/1.1448864.

[14] R. Vijay, J. D. Sau, M. L. Cohen and I. Siddiqi, "Optimizing Anharmonicity in Nanoscale Weak Link Josephson Junction Oscillators", *Phys. Rev. Lett.* 103, p. 087003, 2009, doi: 10.1103/PhysRevLett.103.087003.

[15] R. Vijay, E. M. Levenson-Falk, D. H. Slichter, and I. Siddiqi, "Approaching ideal weak link behaviour with three dimensional aluminum nanobridges", *Appl. Phys. Lett.* 96, p. 223112, 2010, doi: 10.1063/1.3443716.

[16] E.E. Mitchell and S.K.H. Lam, "Niobium dc SQUIDs with Nanobridge Junctions", *Physics Procedia* 36, pp. 382-387, 2012, doi: 10.1016/j.phpro.2012.06.249.

[17] D. Hazra, L. M. A. Pascal, H. Courtois, and A. K. Gupta, "Hysteresis in superconducting short weak links and μ-SQUIDs", *Phys. Rev. B* 82, p. 184530, 2010, doi: 10.1103/PhysRevB.82.184530.

[18] D. Hazra, J. R. Kirtley, and K. Hasselbach, "Retrapping Current in Bridge-Type Nano-SQUIDs", *Phys. Rev. Appl.* 4, p. 024021, 2015, doi: 10.1103/PhysRevApplied.4.024021.

[19] L. Hao, J. C. Macfarlane, J. C. Gallop, D. Cox, J. Beyer, D. Drung, and T. Schurig, "Measurement and noise performance of nano-superconducting-quantum-interference devices fabricated by focused ion beam", *Appl. Phys. Lett.* 92, p. 192507, 2008, doi: 10.1063/1.2917580.

[20] O. W. Kennedy *et al.*, "Tunable Nb superconducting resonator based on a constriction nano-SQUID fabricated with a Ne focused ion beam", *Phys. Rev. Appl*. 11, p. 14006, 2019, doi: 10.1103/PhysRevApplied.11.014006.

[21] K. Uhl, D. Hackenbeck, J. Peter, R. Kleiner, D. Koelle and D. Bothner, "Niobium quantum interference microwave circuits with monolithic three-dimensional nanobridge junctions", *Phys. Rev. Appl.* 21, p. 024051, 2024, doi: 10.1103/PhysRevApplied.21.024051.

[22] K. K. Likharev, "Superconducting Weak Links", *Rev. Mod. Phys.* 51, 101, 1979, doi: 10.1103/RevModPhys.51.101.

[23] W. J. Skocpol, M. R. Beasley, M. Tinkham, "Self-heating hotspots in superconducting thin-film microbridges", *J. Appl. Phys.* 45, pp. 4054–4066, 1974, doi: 10.1063/1.1663912.

[24] A. Blois, S. Rozhko, L. Hao, J. C. Gallop and E. J. Romans, "Proximity effect bilayer nano superconducting quantum interference devices for millikelvin magnetometry", *J. Appl. Phys.* 114 (23), 233907, 2013, doi: 10.1063/1.4843856.

[25] J. O'Gorman *et al*., "A silicon-based surface code quantum computer", *npj Quantum Information* 2, 15019, 2016, doi: 10.1038/npjqi.2015.19.

[26] Proximity effect correction using BEAMER package, GenISys GmbH.

[27] R. Rodrigo, M. I. Faley and R. E. Dunin-Borkowski, "NanoSQUIDs based on Nb nanobridges", *J. Phys.: Conf. Ser*. 1559, 012011, 2020, doi:10.1088/1742-6596/1559/1/012011.

[28] A. G. P. Troeman *et al*., "Temperature dependence measurements of the supercurrent-phase relationship in niobium nanobridges", *Phys. Rev. B* 77, 024509, 2008, doi: 10.1103/PhysRevB.77.024509.

[29] N. Kumar, T. Fournier, H. Courtois, C. B. Winkelmann, and A. K. Gupta, "Reversibility of superconducting Nb weak links driven by the proximity effect in a quantum interference device", *Phys. Rev. Lett.* 114, p. 157003, 2015, doi: 10.1103/PhysRevLett.114.157003.